Theoretical Study of the Mechanism of Palladium(0)-Catalyzed Intramolecular [2+2+2] Cycloaddition of Ester-Substituted Alkynes

Yoshihiko Yamamoto*[a]

[a] Prof. Dr. Y. Yamamoto
Department of Basic Medicinal Sciences
Graduate School of Pharmaceutical Sciences, Nagoya University
Chikusa, Nagoya 464-8601
E-mail: yamamoto-yoshi@ps.nagoya-u.ac.jp
http://www.ps.nagoya-u.ac.jp/lab_pages/molecular_design/yamamoto_lab/index.html

Supporting information for this article is given via a link at the end of the document.((Please delete this text if not appropriate))

WILEY-VCH

Abstract: The mechanisms of the palladium(0)-catalyzed cross [2+2+2] cycloaddition of a diyne diester with dimethyl acetylenedicarboxylate and of the [2+2+2] cyclization of a triyne diester were investigated using density functional theory calculations. After evaluating the kinetic and thermodynamic profiles of each reaction, the roles of the ester substituents on the alkyne substrates and of the triphenylphosphine ligand are discussed based on the obtained results. Moreover, the previously unreported cross [2+2+2] cycloaddition of the diyne diester with nitriles was also investigated, in order to evaluate its feasibility under the relevant experimental conditions.

Introduction

Since the pioneering discovery of the nickel-catalyzed cyclooligomerizations of alkynes by Reppe and coworkers,[1] the transition-metal-catalyzed alkyne [2+2+2] cycloaddition has been extensively developed as a powerful method to synthesize multiply substituted benzene derivatives.[2] In particular, partially or fully intramolecular [2+2+2] cycloadditions of diynes and triynes have been recognized as straightforward approaches to valuable fused benzene derivatives in a single operation.[2] In addition to these synthetic advantages, the transition-metal-catalyzed alkyne [2+2+2] cycloaddition has also attracted considerable attention from a mechanistic point of view.[3] Based on the isolation of metallacyclopentadiene intermediates, Shore proposed the so-called "common mechanism", illustrated in Scheme 1a.[4] Bis(alkyne) complex **A** undergoes oxidative coupling (OC) to produce metallacyclopentadiene intermediate **B**. Subsequent insertion of an alkyne into the M–Cα bond of **B** generates metallacycloheptatriene intermediate **C**. Alternatively, metallanorbornadiene intermediate **D** can be generated through the Diels–Alder-type [4+2] cycloaddition of **B** with an alkyne. Finally, reductive elimination (RE) from **C** or **D** yields the final benzene product, with the concomitant restoration of a catalytically active metal species. Although **C**- and **D**-type intermediates have hardly been observed in catalytic reactions, the "common mechanism" has been accepted as a reasonable pathway on the basis of theoretical investigations of cobalt- and rhodium-catalyzed reactions using density functional theory (DFT) methods.[5,6] On the other hand, the Kirchner and Yamamoto groups independently proposed a new reaction pathway involving ruthenacyclopentatriene intermediate **E**, in which the Ru–Cα distance is similar to that of Ru=C double bonds, and the Cα–Cβ bonds are shorter than the Cβ–Cβ one (Scheme 1b).[7] Related ruthenacyclopentatriene complexes have been isolated and characterized by X-ray crystallography.[7b,8] Because of its biscarbenoid character, **E** undergoes [2+2] cycloaddition with an alkyne to produce ruthenabicycle intermediate **F**. Although this type of metallabicycle complex has not been experimentally observed as a catalytic intermediate, a closely related iridabicycle complex was reported by Paneque and coworkers.[9] The ruthenabicycle intermediate readily undergoes ring opening to generate ruthenacycloheptatetraene intermediate **G**, which then transforms into the final benzene product *via* reductive elimination. In addition to mechanisms involving metallacycle intermediates, sequential insertion and metathesis mechanisms have also been proposed, although they are less common.[10,11]

(a) Shore's "Common mechanism"

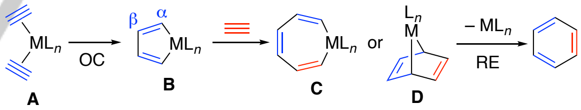

(b) Metallacyclopentatriene mechanism

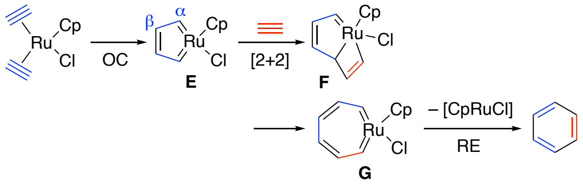

Scheme 1. Mechanisms of transition-metal-catalyzed alkyne cyclotrimerizations involving metallacycle intermediates.

In contrast to Ru, Co, Rh, and Ni catalysts, Pd catalysts have not been extensively explored for alkyne [2+2+2] cycloadditions.[2] In particular, Pd(0)-catalyzed reactions have been limited to those involving electron-deficient alkynes. The Maitlis and Ishii groups independently reported that the reaction of a palladium(0) dibenzylideneacetone (dba) complex with dimethyl acetylenedicarboxylate (DMAD) yielded palladacyclopentadiene **1** in an oligomeric form (Scheme 2a).[12] Although the stoichiometric reaction of **1** with DMAD or diphenylacetylene afforded the corresponding fully substituted benzenes, catalytic cyclotrimerization only occurred with highly activated alkynes such as DMAD, highlighting the importance of electron-withdrawing groups on the alkyne components. Later, Itoh, Yamamoto, and coworkers reported the Pd(0)-catalyzed intramolecular [2+2+2] cycloadditions of electron-deficient alkynes (Scheme 2b).[13] They designed diesters of 1,6-diynes or 1,6,11-triynes as tethered alkyne substrates for intramolecular cycloadditions. In the presence of catalytic amounts of $Pd_2(dba)_3$ and PPh_3 (Pd/PPh_3 = 1:1), diyne diesters **3** reacted with 1.1 equiv of DMAD under toluene reflux to selectively afford fused benzenes **4**. Similarly, cyclization of triyne diesters **5** also produced tricyclic benzenes **6** as exclusive products. The authors prepared oligomeric palladacycle **7a** through the stoichiometric reaction of **3a** (X = O) and $Pd_2(dba)_3$, and the palladacycle formation was confirmed through the X-ray diffraction analysis of monomeric bis(pyridine) complex **7b** derived from **7a**. Palladacycle **7a** could be used as a catalyst for the cycloaddition of **3a** with DMAD, indicating that **7a** is the reaction intermediate. Moreover, the stoichiometric reaction of $Pd_2(dba)_3$ with triyne diester **5a** (X = O) yielded Pd(0) tris(alkyne) complex **8** instead of the expected palladacycles. Upon heating or PPh_3 addition, **8** could be smoothly converted into the corresponding cyclization product (**6a**, X = O).

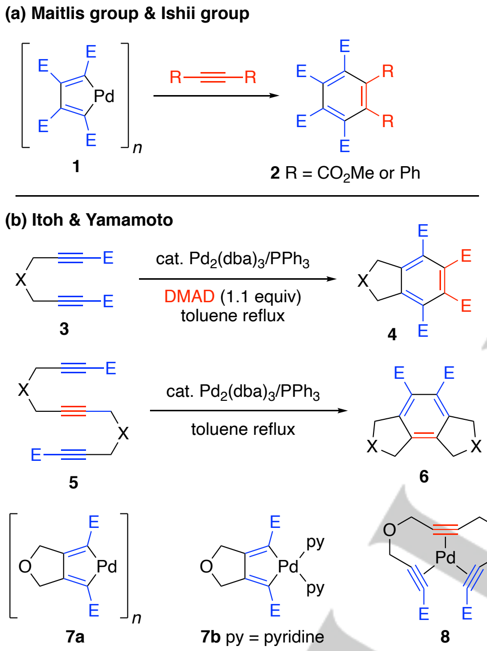

Scheme 2. Pd(0)-mediated [2+2+2] cycloaddition of electron-deficient alkynes (E = CO_2Me).

Accordingly, the Pd(0)-catalyzed [2+2+2] cycloadditions of tethered alkyne esters successfully provide an efficient access to fused benzene esters. However, the detailed mechanisms of these intramolecular cycloadditions remain unclear, although the relevant intermediates have been characterized. This article provides a general outline of the mechanism of Pd(0)-catalyzed intramolecular [2+2+2] cycloadditions based on DFT calculations; in particular, the calculations elucidated the role of the electron-withdrawing groups on the alkyne substrates. Further calculations were performed to assess the feasibility of the previously unreported Pd(0)-catalyzed [2+2+2] cycloaddition of a diyne diester with nitriles.

Computational Methods

The Gaussian 16 program package was used for all calculations.[14] The geometries of the stationary points and transition states were fully optimized using the Becke's three-parameter hybrid density functional method with the Perdew/Wang91 correlation functional (B3PW91),[15] with a [3*s*3*p*2*d*1*f*] contracted-valence basis set with the relativistic effective core potential of Hay and Wadt [LanL2DZ(*f*)][16] for Pd and the 6-31G(d)[17] basis sets for other elements. The D3 version of Grimme's dispersion with Becke–Johnson damping (GD3BJ)[18] was used for empirical dispersion correction. The geometry optimization of X-ray structure of Pd(0) triyne complex **8** afforded structural parameters similar to those obtained by X-ray crystallography (Figure 1). The vibrational frequencies and the thermal correction to Gibbs energy (TCGFE) including the zero-point energy were calculated at the same level of theory. The obtained structures were characterized by the number of imaginary frequencies (IF, one or zero for the transition and ground states, respectively). The connectivity of each step was also confirmed using the intrinsic reaction coordinate (IRC)[19] calculation from the transition states, followed by optimization of the resultant geometries. Single-point energies for geometries obtained using the above method were calculated at the same level of theory using a [6*s*5*p*3*d*2*f*1*g*] contracted-valence basis set with the Stuttgart-Dresden-Bonn energy-consistent pseudopotential (SDD)[20] for Pd and the 6-311++G(d,p) basis sets[21] for other elements. The GD3BJ dispersion correction was also employed. To examine the solvent effect, the above single-point energy calculations were performed using the SMD model[22] with toluene as the solvent. CYLview (Ver. 1.0b)[23] was used for the visualization of the optimized structures.

Selected interatomic distances (Å) and angles (°).

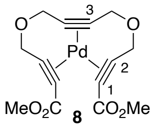

8

	X-ray*	DFT
Pd–C1	2.134 (1)	2.160
Pd–C2	2.145 (1)	2.155
Pd–C3	2.191 (2)	2.199
C1–C2	1.239 (2)	1.250
C3–C3'	1.222 (3)	1.245
Pd–C1–C2	73.64 (9)	72.94
Pd–C2–C1	72.69 (9)	73.38
Pd–C3–C3'	74.0 (1)	73.57

***Refs. 12b,c**

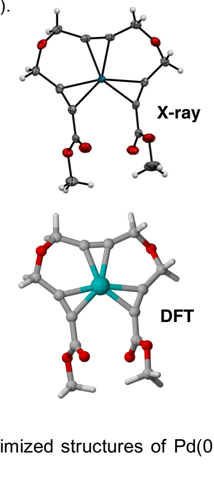

Figure 1. Comparison of X-ray and DFT-optimized structures of Pd(0) triyne complex **8**.

Results and Discussion

Partially intramolecular cycloaddition of diyne diester

(i) Oxidative coupling step. It is remarkable that the selective cross cycloaddition of diyne diesters with DMAD could be achieved using the Pd(0)/PPh_3 catalyst, even though DMAD was employed in a slight excess (1.1 equiv) to the diyne diesters. In general, excess amounts of a monoalkyne are required to suppress the self-cycloaddition of diynes. Moreover, the cyclotrimerization of DMAD is a very facile process; however, the formation of hexamethyl mellitate was effectively suppressed in the cross cycloaddition with diyne diesters. The use of a diyne monoester afforded the corresponding cycloadduct in a yield lower than those of the products derived from diyne diesters, indicating that the ester substituents of the diyne substrates have a significant impact on the Pd(0)-catalyzed cross cycloaddition. To obtain insights into the high cross-selectivity, the first important step of the catalytic cycle, namely, the oxidative coupling leading to palladacycle intermediates, was investigated at the outset.

The oxidative coupling of DMAD from Pd(0) bis(alkyne) complex **9**, bearing bent η^2-alkyne ligands, proceeds *via* **TS$_{9\text{-}10}$** with an activation energy ($\Delta G^{\ddagger}$) of +28.1 kcal/mol, resulting in the exergonic (–23.7 kcal/mol) formation of palladacycle **10** (Scheme 3a).[24] Palladacycle **10** has a metallacyclopentadiene structure with the C1–C2 and C1'–C2' bonds (1.351 and 1.364 Å, respectively) shorter than the C2–C2' bond (1.465 Å). Although **9** adopts a distorted trigonal geometry, as evidenced by the similar values of the P–Pd–C1 and P–Pd–C1' angles (100.1° and 97.4°, respectively), these angles are quite different (∠P–Pd–C1 = 172.5° and ∠P–Pd–C1' = 106.3°) in palladacycle **10**, because of its T-shape geometry. Owing to the strong trans influence from the C1 carbon, the Pd–P bond in **10** (2.389 Å) is longer than that in **9** (2.346 Å). Conversely, the Pd–C1 bond (1.977 Å) is shorter than the Pd–C1' bond (1.996 Å), due to the trans influence from the PPh_3 ligand. The oxidative coupling step for diyne diester complex **11a** is illustrated in Scheme 3b. The obtained geometries of **11a** and **12a** are very similar to those of **9** and **10**, respectively. The activation barrier for **TS$_{11a\text{-}12a}$** is 3.6 kcal/mol smaller than that for **TS$_{9\text{-}10}$**. Moreover, the formation of bicyclic complex **12a** is less exergonic (–19.4 kcal/mol) than that of monocyclic **10**. Thus, the oxidative coupling of the diyne diester is kinetically more efficient but thermodynamically less favored than that of DMAD. In striking contrast, the activation energy for the diyne oxidative coupling shows a substantial increase to +46.5 kcal/mol in the absence of the PPh_3 ligand (see, Scheme S1 in the Supporting Information), highlighting the indispensable role of this ligand.

To shed light on the influence of the ester substituent, the oxidative couplings for diynes with a single ester terminal (series **b**) or without ester terminal (series **c**) were also investigated, and the obtained results were compared to those obtained for the diyne diester (Table 1, also see Schemes S2 and S3 in the Supporting Information). The activation energies increase in the order **11a** < **11b** < **11c** and the exergonicities decrease in the order **11a** > **11b** > **11c**. Accordingly, the ester terminal groups play important roles in lowering the activation barrier for oxidative coupling by lowering the LUMO level of the C–C triple bonds and stabilizing the palladacycles with respect to the corresponding diyne complexes.

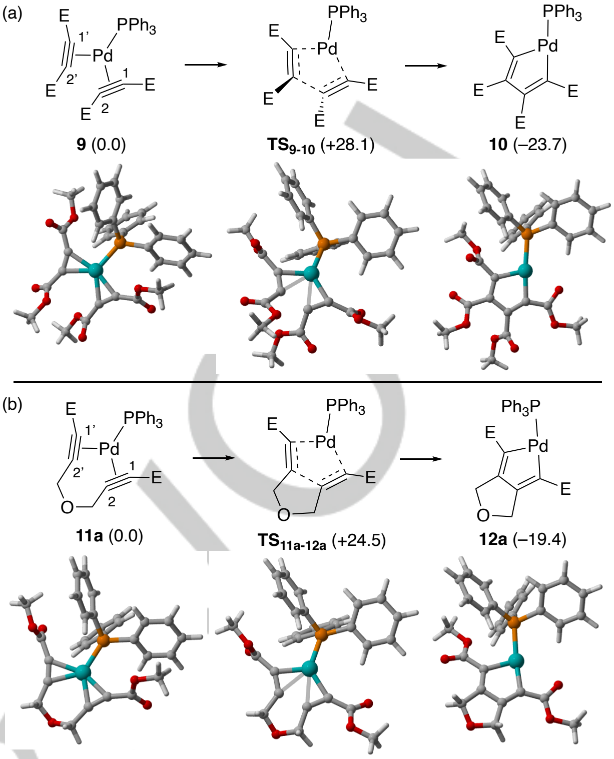

Selected interatomic distances (Å).

	9	TS$_{9\text{-}10}$	10	11a	TS$_{11a\text{-}12a}$	12a
Pd–P	2.346	2.212	2.389	2.328	2.192	2.375
Pd–C1	2.116	2.089	1.977	2.125	2.059	2.001
Pd–C2	2.131	2.267	2.888	2.113	2.276	2.867
Pd–C1'	2.109	2.005	1.996	2.142	2.029	2.013
Pd–C2'	2.111	2.283	2.871	2.113	2.297	2.843
C1–C2	1.253	1.311	1.351	1.258	1.319	1.350
C1'–C2'	1.263	1.305	1.364	1.257	1.306	1.360
C2–C2'	3.127	1.954	1.465	2.878	1.816	1.445

Scheme 3. Oxidative coupling of Pd(0) bis(alkyne) complexes **9** and **11a** (E = CO_2Me). Relative Gibbs energies at 298 K are given in parentheses (kcal/mol).

Table 1. Activation and reaction energies ($\Delta G^{\ddagger}$ and ΔG_{rxn}, respectively) for oxidative coupling step of diyne complexes **11** at 298 K (kcal/mol).

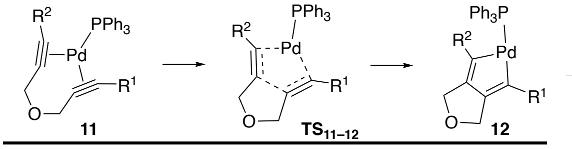

Complexes	$\Delta G^{\ddagger}$	ΔG_{rxn}
11a, $R^1 = R^2 = CO_2Me$	+24.5	-19.4
11b, R^1 = Me, $R^2 = CO_2Me$	+26.1	-14.6
11c, $R^1 = R^2$ = Me	+29.0	-5.9

(ii) Transformation of fused palladacycle 12a. This section focuses on the reaction of palladacycle **12a** with DMAD. Palladacycle **13a**, bearing one DMAD molecule as an η^2 ligand, could be identified as a minimum (Scheme 4). The insertion of DMAD into the adjacent Pd–Cα bond proceeds *via* **TS$_{13a\text{-}14a}$** with an activation energy of +11.3 kcal/mol, affording fused palladacycloheptatriene **14a**, which is 9.1 kcal/mol more stable than **13a**. In contrast to **12a**, the PPh_3 ligand is not coplanar with the almost flat palladacycle moiety in **14a**. The palladacycloheptatriene framework of **14a** is unusual, in the sense that the Pd–C1'–C2' and Pd–C4–C3 angles (ca. 103°) are much smaller than the reported angles for palladium(II) styryl complexes (ca. 129°),[25] and the C1'–Pd–C4 angle (145.7°) is much larger than those of the DFT-optimized metallacycloheptatrienes (less than 100°).[5c,6a] The Pd–Cα bonds (Pd–C4 = 1.963 Å and Pd–C1' = 1.972 Å) are significantly shorter than those observed in palladacyclopentadiene **12a** (Pd–C1 =2.001 Å and Pd–C1' = 2.013 Å) and in the X-ray data of bis(pyridine) complex **7b** (2.041(3) Å). The C=C bond distances within the palladacycloheptatriene framework (1.364–1.383 Å) are similar to those of normal C=C double bonds. Subsequent reductive elimination proceeds *via* **TS$_{14a\text{-}15}$** with a very small activation energy (+1.4 kcal/mol), and the formation of Pd(0) η^2-arene complex **15** from **14a** is highly exergonic (–74.7 kcal/mol). Therefore, this step is highly favorable from both kinetic and thermodynamic viewpoints.

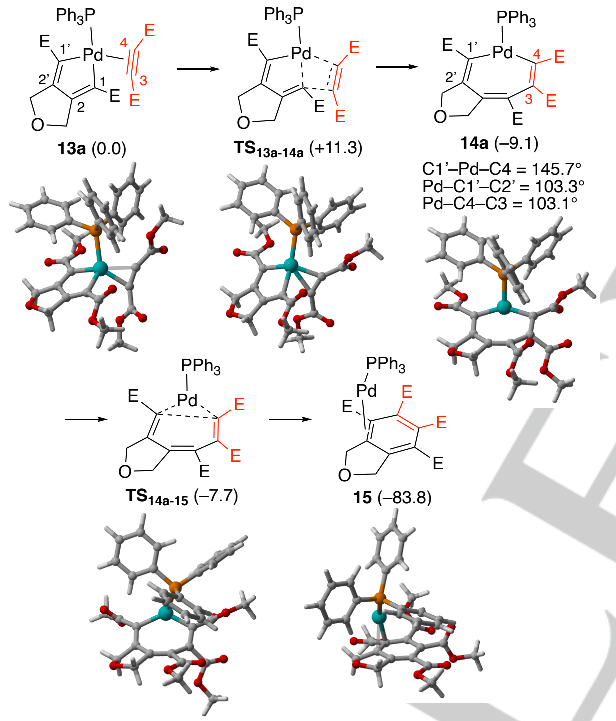

Selected interatomic distances (Å).

	13a	**TS$_{13a\text{-}14a}$**	**14a**	**TS$_{14a\text{-}15}$**	**15**
Pd–P	2.386	2.310	2.193	2.207	2.270
Pd–C1	2.054	2.106	2.913	3.057	3.469
Pd–C2	2.898	2.853	2.920	3.114	2.930
Pd–C1'	2.017	2.041	1.972	2.061	2.171
Pd–C2'	2.881	2.847	2.643	2.813	2.225
Pd–C3	2.117	2.190	2.633	2.696	3.349
Pd–C4	2.208	2.089	1.963	1.925	2.730
C1–C2	1.354	1.368	1.383	1.376	1.389
C1'–C2'	1.357	1.361	1.364	1.360	1.421
C2–C2'	1.431	1.434	1.489	1.474	1.414
C1–C3	2.877	2.052	1.501	1.495	1.422
C3–C4	1.256	1.289	1.365	1.348	1.388
C1'–C4	4.123	3.942	3.761	3.577	1.441

Scheme 4. DMAD insertion and subsequent reductive elimination steps from palladacyclopentadiene **13a** (E = CO_2Me). Relative Gibbs energies at 298 K are given in parentheses (kcal/mol).

To gain further insight into the effect of electron-withdrawing groups on monoalkyne components, the insertions of methyl butynoate and 2-butyne were also investigated (Table 2, also see Schemes S4 and S5 in the Supporting Information). The results show that the insertion steps of these alkynes are similar to that of DMAD. However, the activation barriers increase in the order **13a** < **13b** < **13c**, highlighting the importance of the ester substituents. It can be assumed that the ester groups act as electron-withdrawing groups to enhance the back-donation from the Pd center to the coordinated alkyne moiety. In fact, the Pd–C3 and Pd–C4 distances are longer in **13b** and **13c** than in **13a**. The C3–C4 bond length in **13a** is longer (1.256 Å) than those in **13b** and **13c** (1.226 Å). Moreover, the exergonicities decrease in the order **14a** > **14b** > **14c**. Therefore, the insertion of highly activated DMAD is both kinetically and thermodynamically more favorable than those of methyl butynoate and 2-butyne. Accordingly, the cross cycloaddition of a diyne diester with DMAD is more efficient than the cyclodimerization of two diyne diester molecules. The cross cycloaddition of a diyne diester with an unactivated internal alkyne is difficult to achieve, because it should be less favorable than the cyclodimerization of diyne diesters.

Table 2. Activation and reaction energies (ΔG‡ and ΔG$_{rxn}$, respectively) for insertion step from **13** at 298 K (kcal/mol) and related interatomic distances (Å) in **13** (E = CO_2Me).

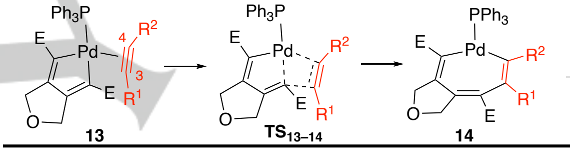

Complexes	ΔG‡	ΔG$_{rxn}$	Pd–C3/Pd–C4/C3–C4
13a, $R^1 = R^2 = CO_2Me$	+11.3	-9.1	2.117/2.208/1.256
13b, $R^1 = CO_2Me$, $R^2 = Me$	+14.3	-1.6	2.271/2.617/1.226
13c, $R^1 = R^2 = Me$	+17.9	+4.5	2.307/2.490/1.226

Next, the Diels–Alder-type [4+2] cycloaddition pathway was examined, and the obtained results are outlined in Scheme 5. Cycloaddition proceeds from palladacycle **16**, in which DMAD is coordinated to the Pd center with one of the ester carbonyl groups. *O*-Bound DMAD complex **16** is 5.2 kcal/mol less stable than η^2-DMAD complex **13a**. The transition state **TS$_{16\text{-}17}$** is asynchronous, as evidenced by the significantly different incipient bond lengths (C1–C3 = 2.212 Å and C1'–C4 = 2.328 Å). The corresponding activation energy (+19.2 kcal/mol) is much higher than that of the insertion pathway (**13a** → **14a**, ΔG‡ = +11.3 kcal/mol). Therefore, the Diels–Alder-type pathway is kinetically disfavored with respect to the insertion pathway, although the formation of palladanorbornadiene **17** from **16** is exergonic by 27.9 kcal/mol, and thus, thermodynamically more favorable than the formation of palladacycloheptatriene **14a** from **13a** (exoergonic by 9.1 kcal/mol).

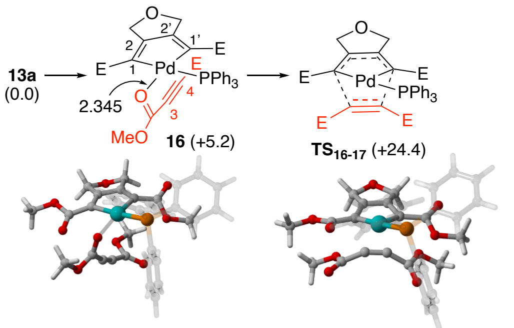

Selected interatomic distances (Å).

	16	$TS_{16\text{-}17}$	17
Pd–P	2.357	2.352	2.308
Pd–C1	2.068	2.008	2.145
Pd–C2	2.872	2.892	2.934
Pd–C1'	2.002	2.015	2.159
Pd–C2'	2.836	2.872	2.897
Pd–C3	2.955	2.997	2.712
Pd–C4	3.195	2.977	2.669
C1–C2	1.357	1.391	1.500
C1'–C2'	1.357	1.400	1.514
C2–C2'	1.445	1.395	1.333
C1–C3	3.558	2.212	1.528
C3–C4	1.211	1.250	1.354
C1'–C4	3.998	2.328	1.542

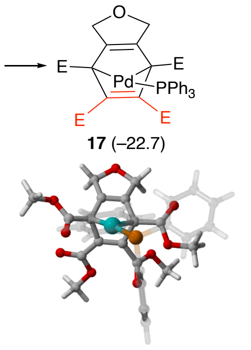

Scheme 5. Diels–Alder-type reaction of palladacycle **16** (E = CO_2Me). Relative Gibbs energies at 298 K are given in parentheses (kcal/mol).

(iii) Overall reaction profile for insertion pathway. Figure 2 shows the energy surface for the overall transformation of diyne diester complex **11a** into η^2-arene complex **15** along the insertion pathway. The most difficult step is the initial oxidative coupling; however, the highest activation barrier with $\Delta G^{\ddagger}$ = +24.5 kcal/mol can be overcome under the relevant experimental conditions (toluene reflux). The formation of palladacyclopentadiene **12a** is exergonic by 19.4 kcal/mol, which is slightly less stable than its conformer **12a'**. The coordination of DMAD generates **13a**, which is more stable than **12a** and **12a'**. The subsequent insertion of coordinated DMAD is easier because of the much lower activation barrier ($\Delta G^{\ddagger}$ = +11.3 kcal/mol). Moreover, the final reductive elimination step from palladacycloheptatriene intermediate **14a** is almost barrierless ($\Delta G^{\ddagger}$ = +1.4 kcal/mol). The formation of η^2-arene complex **15** from diyne diester complex **11a** is highly exergonic (–111.5 kcal/mol) due to the benzene-ring formation, indicating that the overall reaction is thermodynamically very favorable. Because, in general, η^2-arene ligands are very labile and electron-deficient alkynes are good ligands for the Pd(0)PPh_3 fragment, the restoration of **11a** from **15** and the diyne diester is very facile (ΔG_{rxn} = – 30.3 kcal/mol, see Scheme S6 in the Supporting Information). Thus, the catalytic cycle should readily turnover.

Fully intramolecular cycloaddition of triyne diester

(i) Cyclization without PPh_3. The isolated triyne complex **8** underwent [2+2+2] cyclization even at room temperature in a $CDCl_3$ solution to produce tricyclic benzene product **6a** (X = O).[13c] Thus, this section focuses on the cyclization of the triyne complex without the PPh_3 ligand. Two oxidative coupling pathways are possible for triyne complex **19**, which is 1.6 kcal/mol more stable than solid-state conformer **8**: one involves the two activated alkyne terminals (blue), while the other takes place between one of the activated alkyne terminals and the internal unactivated alkyne moiety (red). The efficiency of these two oxidative coupling steps was first evaluated (Scheme 6). The activation barrier of the oxidative coupling between the two alkynoate terminals (**TS**$_{19\text{-}20}$, $\Delta G^{\ddagger}$ = +52.4 kcal/mol) is too high to overcome under the relevant experimental conditions. Moreover, the formation of palladacycle **20** (with the free internal alkyne moiety) from **19** is slightly endergonic (+4.8 kcal/mol). Therefore, this type of oxidative coupling is both kinetically and thermodynamically infeasible. The inefficiency of this process can be ascribed to the energetic penalty associated with the formation of a strained cyclophane-type 12-membered cyclyne framework. On the other hand, oxidative coupling between one of the alkynoate terminals and the internal alkyne moiety proceeds *via* **TS**$_{19\text{-}21}$ with a much lower activation energy (+24.4 kcal/mol), and the formation of palladacyclopentadiene **21** (with the coordinated alkynoate terminal) from **19** is exergonic by 12.6 kcal/mol. Accordingly, the latter oxidative coupling is much more efficient than the former.

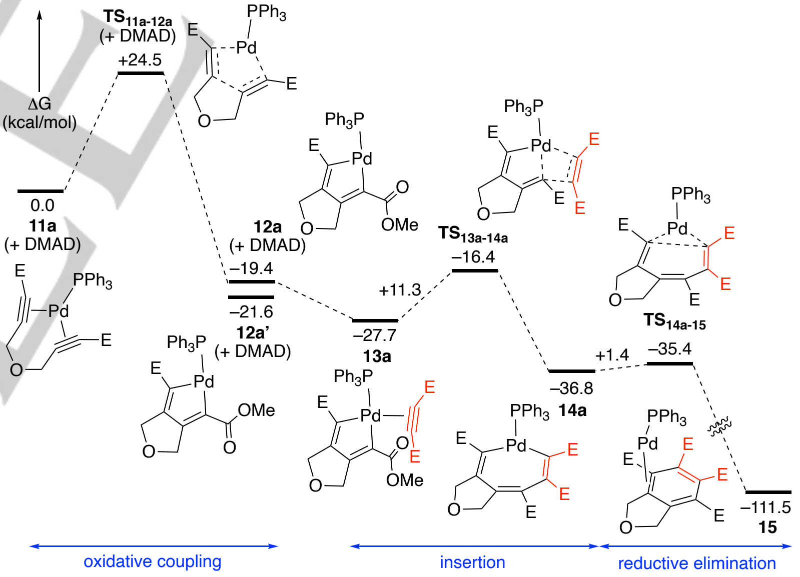

Figure 2. Energy surface for transformation of diyne complex **11a** into η^2-arene complex **15** with relative Gibbs energies at 298 K (E = CO_2Me).

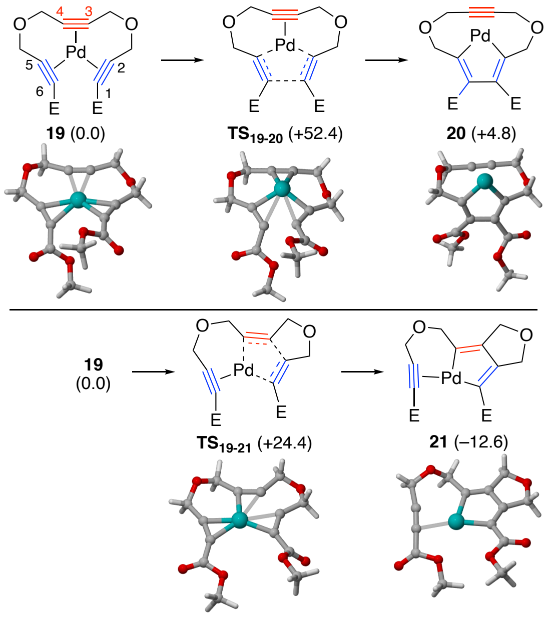

Selected interatomic distances (Å).

	19	**TS_{19-20}**	**20**	**TS_{19-21}**	**21**
Pd–C1	2.144	2.315	2.826	2.086	2.012
Pd–C2	2.142	2.003	1.960	2.308	2.842
Pd–C3	2.205	2.052	3.054	2.314	2.838
Pd–C4	2.206	2.024	3.052	2.006	2.010
Pd–C5	2.142	2.055	1.975	2.035	2.453
Pd–C6	2.144	2.432	2.831	2.056	2.326
C1–C2	1.253	1.313	1.358	1.303	1.354
C2–C3	2.914	2.959	2.904	1.853	1.442
C3–C4	1.243	1.272	1.214	1.295	1.347
C4–C5	2.914	2.975	2.996	2.800	3.085
C5–C6	1.253	1.305	1.358	1.273	1.225
C1–C6	3.110	1.881	1.463	3.595	4.295

Scheme 6. Oxidative coupling of Pd(0) triyne complex **19** leading to palladacycles **20** or **21** (E = CO_2Me). Relative Gibbs energies at 298 K are given in parentheses (kcal/mol).

As the next step, the insertion of a pendant alkynoate terminal into the Pd–Cα bond of palladacycle **21** was investigated and the transition state for the intramolecular [2+2] cycloaddition, leading to palladatricycle intermediate **22**, was found as shown in Scheme 7. The activation energy of this step is +23.2 kcal/mol, which is slightly lower than that of the initial oxidative coupling step. Palladatricycle **22** is 5.2 kcal/mol less stable than palladacyclopentadiene **21**. Subsequent scission of the Pd–C4 bond of **22** occurs *via* $\mathbf{TS_{22-23}}$ with a very low activation energy (+4.5 kcal/mol), producing planar and symmetrical palladacycloheptatriene intermediate **23**, which is considerably different from palladacycle **14a** derived from the diyne diester and DMAD (Scheme 4). Because of its highly delocalized structure, as evidenced by the short Pd–Cα bonds (1.928 Å) and similar C–C bond lengths (1.355–1.442 Å) within the pallladacycle, **23** is much more stable than **21** and **22**. The reductive elimination step from **23** proceeds *via* $\mathbf{TS_{23-24}}$ with an activation energy of +19.5 kcal/mol to generate Pd(0) η^2-arene complex **24** as the final product. This step is also exergonic by 21.4 kcal/mol.

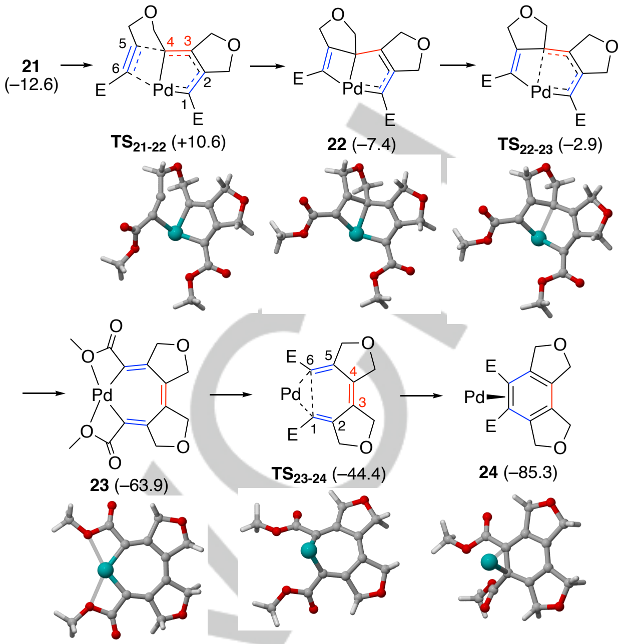

Selected interatomic distances (Å).

	TS_{21-22}	**22**	**TS_{22-23}**	**23**	**TS_{23-24}**	**24**
Pd–C1	1.974	1.949	2.003	1.928	1.972	2.116
Pd–C2	2.775	2.786	2.788	3.051	2.948	2.800
Pd–C3	2.789	2.799	2.866	3.668	3.452	3.447
Pd–C4	2.016	2.070	2.273	3.668	3.452	3.538
Pd–C5	2.648	2.544	2.546	3.051	2.948	3.006
Pd–C6	2.167	2.068	1.966	1.928	1.972	2.224
C1–C2	1.379	1.418	1.405	1.355	1.361	1.422
C2–C3	1.407	1.362	1.374	1.441	1.436	1.384
C3–C4	1.386	1.468	1.441	1.362	1.360	1.394
C4–C5	2.119	1.520	1.510	1.441	1.436	1.384
C5–C6	1.261	1.332	1.329	1.355	1.361	1.419
C1–C6	3.657	3.636	3.327	3.001	2.385	1.454

Scheme 7. Two-step alkyne insertion from palladacyclopentadiene **21** and subsequent reductive elimination from palladacycloheptatriene **23** (E = CO_2Me). Relative Gibbs energies at 298 K are given in parentheses (kcal/mol).

The energy surface for the overall transformation of triyne complex **19** into η^2-arene complex **24**, involving the two-step insertion pathway, is shown in Figure 3. The most difficult step is the initial oxidative coupling from **19**, which exhibits the highest activation barrier ($\Delta G^\ddagger$ = +24.4 kcal/mol). The subsequent [2+2] cycloaddition of **21** is the second most difficult step, with a slightly lower activation barrier ($\Delta G^\ddagger$ = +23.2 kcal/mol). The following opening of the palladabicyclic ring of **22** is much more facile, with a very small activation barrier ($\Delta G^\ddagger$ = 4.5 kcal/mol), and the resulting palladacycloheptatriene **23** is highly stabilized by its delocalized structure. The last reductive elimination step from **23** is also efficient, with an activation energy as high as 20 kcal/mol. The formation of η^2-arene complex **24** from the starting triyne complex **19** is highly exergonic (–85.3 kcal/mol), indicating that the overall reaction is thermodynamically favorable.

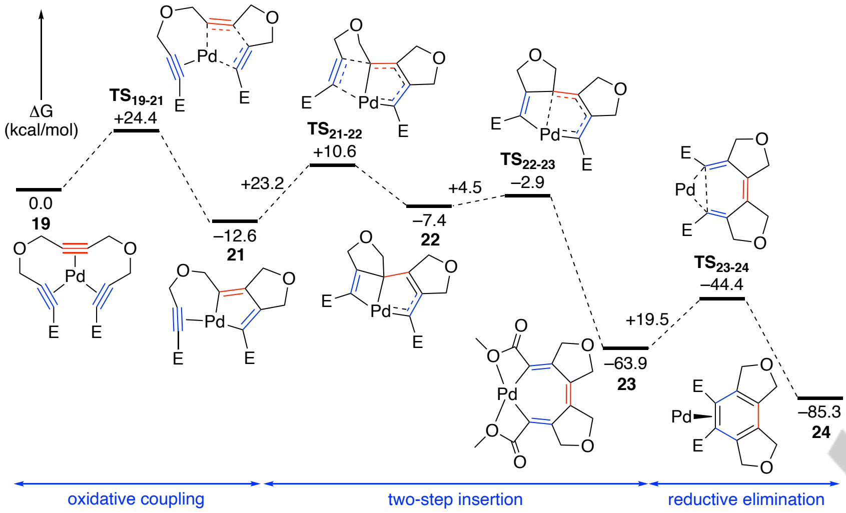

Figure 3. Energy surface for transformation of triyne complex **19** into η^2-arene complex **24** with relative Gibbs energies at 298 K (E = CO_2Me).

(ii) Cyclization in the presence of PPh₃. Although the cyclization of triyne diesters proceeded catalytically in the absence of a ligand, the addition of PPh_3 significantly facilitated the catalytic cyclization.[13c] This section examines the cyclization of the triyne complex with PPh_3. The dissociation of one terminal alkynoate from triyne complex **19** with PPh_3 generates diyne complex **25** with a pendant alkynoate moiety (Scheme 8). The latter is 6.8 kcal/mol more stable than **19**. The oxidative coupling of **25** proceeds *via* **TS$_{25\text{-}26}$** with an activation energy of +23.1 kcal/mol, which is 1.3 kcal/mol lower than the activation energy for the oxidative coupling without the phosphine ligand (**TS$_{19\text{-}21}$**, $\Delta G^\ddagger$ = +24.4 kcal/mol, Scheme 6). The formation of palladacyclopentadiene PPh_3 complex **26** from **25** is exergonic by 17.6 kcal/mol. This value is also higher than the exergonicity of the corresponding process without PPh_3 (**19** → **21**, ΔG_{rxn} = −12.6 kcal/mol, Scheme 6). These data clearly indicate that the PPh_3 ligand facilitates the oxidative coupling step from both kinetic and thermodynamic viewpoints.

In the palladacycle intermediate **26**, the phosphine ligand is located in trans position relative to the ester-substituted carbon (C1), which inhibits the insertion of the pendant alkyne into the adjacent Pd–C4 bond. Thus, the intramolecular Diels–Alder pathway from **26** was investigated as shown in Scheme 8, and a highly asynchronous Diels–Alder transition state (**TS$_{26\text{-}27}$**) could be found. The incipient bond lengths in **TS$_{26\text{-}27}$** are significantly different, as the C1–C6 distance (2.925 Å) is much longer than the C4–C5 one (1.896 Å). This difference is more pronounced than that in the intermolecular Diels–Alder transition state (**TS$_{16\text{-}17}$**, Scheme 5). Nevertheless, the activation barrier for this step ($\Delta G^\ddagger$ = +12.1 kcal/mol) is much lower than that for the intermolecular Diels–Alder process ($\Delta G^\ddagger$ = +19.2 kcal/mol). In striking contrast to the intermolecular reaction, η^2-arene complex **27**, with the Pd(PPh_3) fragment bound to the C3=C4 bond, is directly generated in the process, instead of a palladanorbornadiene intermediate corresponding to **17**.

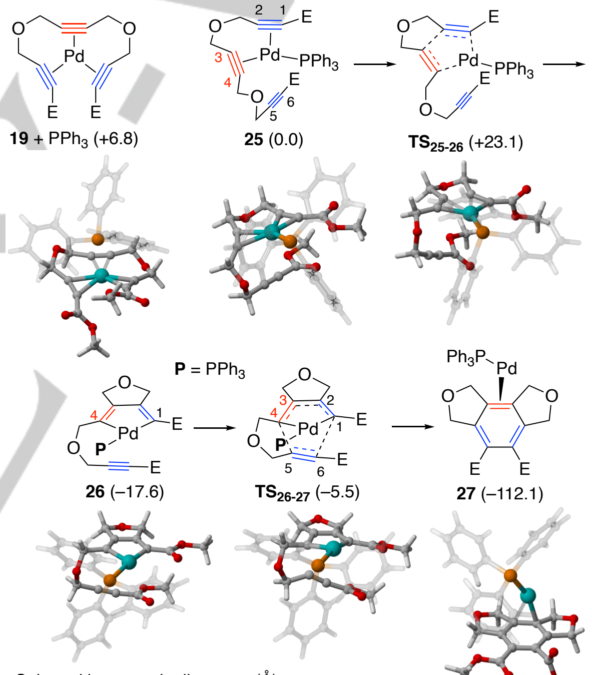

Selected interatomic distances (Å).

	25	TS$_{25\text{-}26}$	26	TS$_{26\text{-}27}$	27
Pd–P	2.339	2.202	2.382	2.372	2.265
Pd–C1	2.106	2.091	2.013	2.005	3.265
Pd–C2	2.089	2.295	2.860	2.888	2.725
Pd–C3	2.150	2.283	2.837	2.864	2.199
Pd–C4	2.165	2.028	2.006	2.026	2.255
Pd–C5	3.266	3.592	3.415	2.811	2.855
Pd–C6	3.184	3.486	3.343	3.123	3.343
C1–C2	1.266	1.306	1.352	1.371	1.383
C2–C3	2.909	1.845	1.446	1.405	1.421
C3–C4	1.251	1.307	1.351	1.401	1.409
C4–C5	3.014	2.923	2.837	1.896	1.416
C5–C6	1.211	1.210	1.210	1.254	1.394
C1–C6	3.746	4.482	3.667	2.925	1.421

Scheme 8. Oxidative coupling step from Pd(0) diyne complex **25** and subsequent Diels–Alder-type reaction of palladacyclopentadiene **26** (E = CO_2Me). Relative Gibbs energies at 298 K are given in parentheses (kcal/mol).

The energy surface for the overall transformation of diyne complex **25** into η^2-arene complex **27**, involving the intramolecular Diels–Alder step, is shown in Figure 4. The most difficult step is the initial oxidative coupling of **25**, showing the highest activation barrier ($\Delta G^{\ddagger}$ = +23.1 kcal/mol), which can be overcome under the relevant experimental conditions. The subsequent intramolecular Diels–Alder cycloaddition of **26** is more facile, because of the much lower activation barrier ($\Delta G^{\ddagger}$ = +12.1 kcal/mol). Remarkably, this intramolecular Diels–Alder process directly produces thermodynamically highly stable η^2-arene complex **27,** with high exergonicity (–112.1 kcal/mol) with respect to **25**. Thus, the overall reaction is both kinetically and thermodynamically favorable.

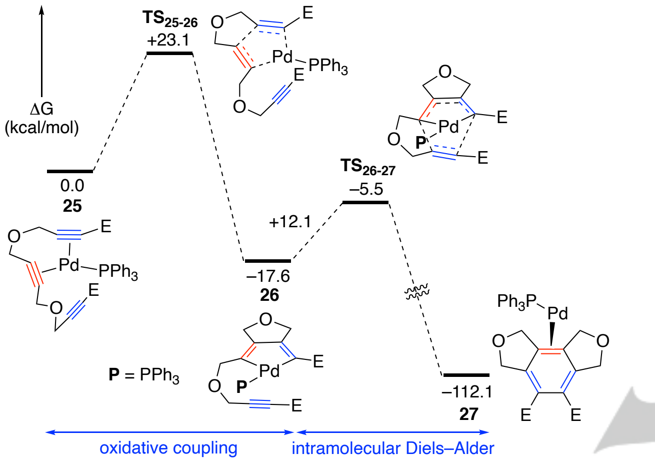

Figure 4. Energy surface for transformation of diyne complex **25** into η^2-arene complex **27** with relative Gibbs energies at 298 K (E = CO_2Me).

Cycloaddition of diyne diester with nitriles

The transition-metal-catalyzed [2+2+2] cocycloaddition of alkynes and nitriles is a powerful approach to substituted pyridines.[26] Therefore, since the seminal studies of Co-catalyzed reactions by the Bönnemann group as well as by Wakatsuki and Yamazaki,[27] a variety of catalyst systems have been developed and applied to the synthesis of natural products and materials. Despite these advances, the Pd(0)-catalyzed alkyne–nitrile [2+2+2] cocycloaddition has remained undeveloped until the recent studies by Mulcahy and coworkers.[28] These authors have achieved the short-step synthesis of fused carbolines through the Pd(0)-catalyzed fully intramolecular [2+2+2] cocycloadditions of diyne–nitrile substrates, including aniline tethers. However, the intermolecular [2+2+2] cycloaddition of diynes with nitriles remains elusive, to the best of our knowledge. In this section, the Pd(0)/PPh_3-catalyzed reaction of a diyne diester with nitriles is discussed based on the results of DFT calculations.

As the first step, the reaction of methyl cyanoformate as an activated nitrile with palladacyclopentadiene **12a** was investigated for comparison with that of DMAD. In the case of nitriles, the η^1 endo-on coordination is generally preferred over the η^2 side-on one.[29] In fact, no η^2-nitrile complex could be located; instead, palladacycle **12a** with a free cyanoformate was located 9.0 kcal/mol above palladacycle **28a** with an *N*-bound nitrile ligand (Scheme 9). The transition state for insertion of the nitrile into the adjacent Pd–Cα bond was searched for; however, [2+2] cycloaddition transition state **TS$_{28a–29a}$** was found, with azapalladacycle intermediate **29a** as the product. The activation energy for this process is +23.8 kcal/mol, which is much higher than those of the alkyne insertions shown in Table 2 ($\Delta G^{\ddagger}$ = +11.3–17.9 kcal/mol). Because alkynes behave as η^2-ligands, their insertion into the metallacyclopentadienes can proceed with smaller ligand motions than that of η^1-nitrile ligands. Actually, the C1–C3 distance in **28a** (3.951 Å) is much larger than that in **TS$_{28a–29a}$** (1.935 Å). Therefore, the transformation of **28a** into **TS$_{28a–29a}$** has a large energetic penalty arising from an extensive structural deformation. Moreover, the formation of **29a** from **28a** is 13.9 kcal/mol endergonic and thus, thermodynamically disfavored. This endergonicity can be ascribed to the ring strain of the azapalladabicyclo[3.2.0] framework as well as the stability of **28a**.

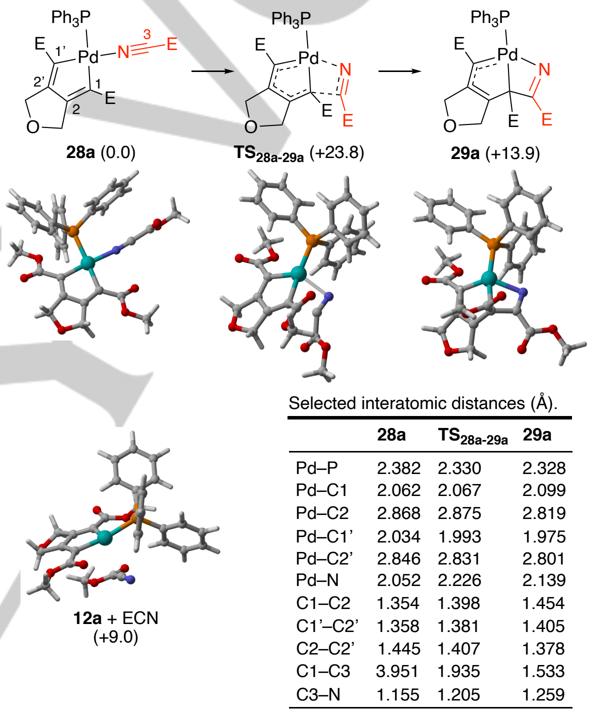

Selected interatomic distances (Å).

	28a	TS$_{28a-29a}$	29a
Pd–P	2.382	2.330	2.328
Pd–C1	2.062	2.067	2.099
Pd–C2	2.868	2.875	2.819
Pd–C1'	2.034	1.993	1.975
Pd–C2'	2.846	2.831	2.801
Pd–N	2.052	2.226	2.139
C1–C2	1.354	1.398	1.454
C1'–C2'	1.358	1.381	1.405
C2–C2'	1.445	1.407	1.378
C1–C3	3.951	1.935	1.533
C3–N	1.155	1.205	1.259

Scheme 9. [2+2] Cycloaddition step from palladacyclopentadiene **28a** (E = CO_2Me). Relative Gibbs energies at 298 K are given in parentheses (kcal/mol).

The influence of nitrile substituents was also examined by evaluating the [2+2] cycloaddition of palladacycles **28b** and **28c** with *N*,*N*-dimethylcyanamide or MeCN as the η^1-nitrile ligand (Table 3, also see Schemes S7 and S8 in the Supporting Information). The [2+2] cycloaddition of **28b** with the electron-rich cyanamide ligand was found to be kinetically and thermodynamically less efficient than that of **28a** involving the electron-deficient cyanoformate, with the activation energy and endergonicity 5.8 and 1.4 kcal/mol higher for the former reaction, respectively. Furthermore, the corresponding reaction involving electronically neutral acetonitrile was found to be much less efficient, as shown by an increased activation energy (+33.6 kcal/mol) and endergonicity (+28.9 kcal/mol). Therefore, the electron-deficient cyanoformate is the most efficient nitrile among those evaluated in this study.

Next, the analysis of the Diels–Alder-type [4+2] cycloaddition of palladacyclopentadiene **28a** with the cyanoformate ligand showed the direct formation of an η^2-pyridine complex (Scheme 10). The [4+2] cycloaddition proceeds *via* **TS$_{28a–30a}$** with an activation energy of +31.5 kcal/mol, which is much higher than that of the insertion pathway (**28a** → **29a**, ΔG‡ = +23.8 kcal/mol). Therefore, the Diels–Alder-type pathway is kinetically disfavored compared with the insertion one, although the formation of η^2-pyridine complex **30a** from **28a** is highly exergonic (–50.4 kcal/mol) and, thus, thermodynamically favored. It is worth noting that the C–C and C–N bond formations are highly asynchronous in **TS$_{28a–30a}$**, as the C1–C3 distance is much shorter than the C1'–N one (1.933 and 2.352 Å, respectively). Similar Diels–Alder-type pathways were found for the reactions of palladacycles **28b** and **28c** with *N*,*N*-dimethylcyanamide or MeCN as the η^1-nitrile ligand (Table S1 and Schemes S9 and S10 in the Supporting Information), although the activation energies are much higher than that obtained for the corresponding reaction of **28a**. The formation of **30b** has comparable exergonicity to that of **30a**, while the formation of **30c** is much less exergonic.

Table 3. Activation and reaction energies (ΔG‡ and ΔG$_{rxn}$, respectively) for [2+2] cycloaddition step from **28** at 298 K (kcal/mol) and related interatomic distances (Å) in **TS$_{28–29}$** (E = CO$_2$Me).

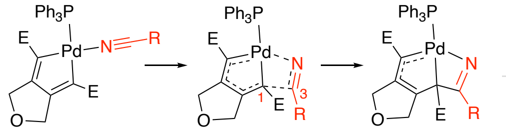

28 **TS$_{28–29}$** **29**

Complexes	ΔG‡	ΔG$_{rxn}$	Pd–N/C1–C3/C3–N
28a, R = CO$_2$Me	+23.8	+13.9	2.226/1.935/1.205
28b, R = NMe$_2$	+29.6	+15.3	2.080/1.963/1.226
28c, R = Me	+33.6	+28.9	2.167/1.896/1.213

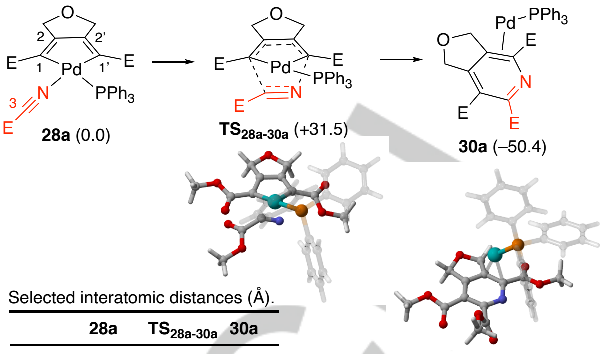

Selected interatomic distances (Å).

	28a	**TS$_{28a-30a}$**	**30a**
Pd–P	2.382	2.324	2.271
Pd–C1	2.062	2.059	3.351
Pd–C2	2.868	2.884	2.812
Pd–C1'	2.034	2.001	2.202
Pd–C2'	2.846	2.856	2.202
Pd–N	2.052	2.956	2.897
C1–C2	1.354	1.405	1.394
C1'–C2'	1.358	1.391	1.423
C2–C2'	1.445	1.392	1.408
C1–C3	3.951	1.933	1.423
C3–N	1.155	1.208	1.316
C1'–N	4.077	2.352	1.363

Scheme 10. Diels–Alder-type reaction of palladacycle **28a** (E = CO$_2$Me). Relative Gibbs energies at 298 K are given in parentheses (kcal/mol).

The kinetic infeasibility of the above Diels–Alder-type pathway can be ascribed to the drastic structural changes from the stable and coordinatively saturated palladacyclopentadiene (**28**) with an η^1-nitrile ligand to the [4+2] transition state (**TS$_{28–30}$**). Palladacycles **28b** and **28c**, with an electron-donating nitrile ligand, should be more stable than **28a**, with the electron-deficient cyanoformate ligand. Accordingly, the transformations of **28b** and **28c** involve much higher activation barriers than for that of **28a**. Thus, the Diels–Alder reaction of palladacycle **28a**, bearing an η^1-cyanoformate ligand, with an extra cyanoformate molecule (**31** → **32**) was investigated, and the obtained results are outlined in Scheme 11. The estimated activation barrier (**TS$_{31–32}$**, ΔG‡ = +21.3 kcal/mol) is much lower than that of the conversion of **28a** into **30a** (ΔG‡ = +31.5 kcal/mol). Thus, this process is kinetically more favorable. Moreover, the formation of η^2-pyridine complex **32**, with an η^2-nitrile ligand, is highly exergonic (–44.9 kcal/mol). Therefore, the [2+2+2] cycloaddition of a diyne diester with cyanoformate is expected to proceed *via* a Diels–Alder pathway involving two nitrile molecules.

WILEY-VCH

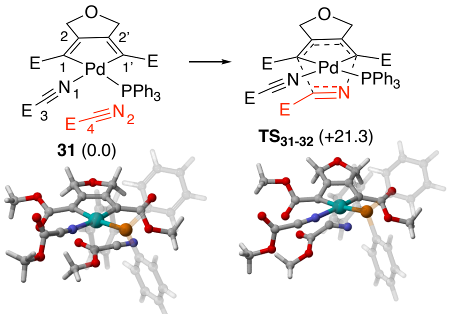

Selected interatomic distances (Å).

	31	TS_{31-32}	32
Pd–P	2.378	2.309	2.287
Pd–C1	2.062	2.132	3.749
Pd–C2	2.870	2.892	3.813
Pd–C1'	2.027	2.015	2.303
Pd–C2'	2.846	2.859	3.202
Pd–N1	2.054	2.061	2.622
Pd–C3	3.200	3.137	2.226
C1–C2	1.355	1.403	1.410
C1'–C2'	1.358	1.390	1.415
C2–C2'	1.444	1.393	1.375
C3–N1	1.155	1.157	1.181
C1–C4	4.228	2.005	1.397
C4–N2	1.161	1.205	1.343
C1'–N2	3.580	2.321	1.372

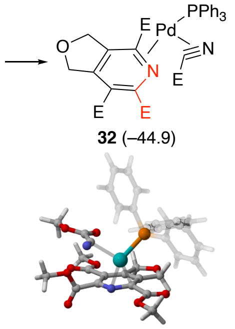

Scheme 11. Diels–Alder-type reaction of palladacycle **31** leading to η^2-pyridine complex **32** (E = CO_2Me). Relative Gibbs energies at 298 K are given in parentheses (kcal/mol).

Finally, the intramolecular Diels–Alder-type reaction of palladacycle **33** with a pendant nitrile was investigated for comparison with the above intermolecular reactions (Scheme 12). The intramolecular [4+2] cycloaddition of the palladacyclopentadiene moiety with a C–N triple bond proceeds *via* highly asynchronous transition state **TS_{26-27}** (C1–N = 2.405 Å and C4–C5 1.756 Å), and the difference between the incipient bond lengths is more pronounced than that observed in the corresponding intermolecular transition state (**$TS_{28c-30c}$**, Table S1). The activation barrier ($\Delta G^{\ddagger}$ = +24.0 kcal/mol) is much lower than those estimated for the intermolecular variants involving one nitrile molecule ($\Delta G^{\ddagger}$ = +31.5–47.1 kcal/mol). The formation of η^2-pyridine complex **34**, with the $Pd(PPh_3)$ fragment bound to the C3=C4 bond, is highly exergonic (–58.3 kcal/mol). Therefore, the intramolecular Diels–Alder pathway starting from **33** is both kinetically and thermodynamically facile, even though the cyano group is unactivated.

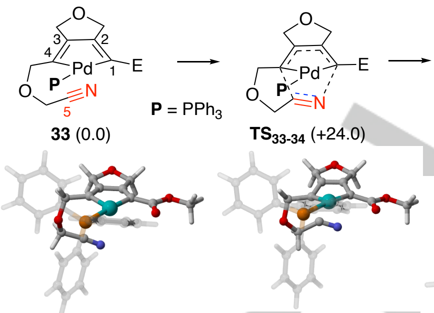

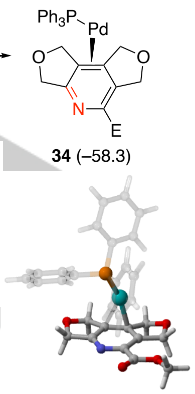

Selected interatomic distances (Å).

	33	TS_{33-34}	34
Pd–P	2.380	2.352	2.272
Pd–C1	1.997	2.014	3.151
Pd–C2	2.866	2.905	2.623
Pd–C3	2.845	2.877	2.182
Pd–C4	2.014	2.046	2.280
Pd–C5	3.579	2.674	2.868
Pd–N	3.738	2.954	3.306
C1–C2	1.348	1.389	1.396
C2–C3	1.448	1.386	1.426
C3–C4	1.353	1.423	1.405
C4–C5	2.909	1.756	1.422
C5–N	1.161	1.218	1.313
C1–N	3.815	2.405	1.359

Scheme 12. Intramolecular Diels–Alder-type reaction of palladacycle **33** leading to η^2-pyridine complex **34** (E = CO_2Me). Relative Gibbs energies at 298 K are given in parentheses (kcal/mol).

Conclusion

The palladium(0)-catalyzed cross [2+2+2] cycloaddition of a diyne diester with DMAD and the [2+2+2] cyclization of a triyne diester were investigated using DFT calculations. The cross cycloaddition of the diyne diester with DMAD proceeds *via* the rate-determining oxidative coupling of the diyne diester to produce a palladacyclopentadiene intermediate, which undergoes insertion of DMAD to generate a palladacycloheptatriene intermediate with an unusual geometry. The final reductive elimination gives rise to an η^2-arene complex with high exergonicity. The overall reaction is both kinetically and thermodynamically feasible under the experimental conditions (toluene reflux). The ester groups on the diyne and monoalkyne substrates play an important role in facilitating the initial oxidative coupling and subsequent insertion steps.

In the absence of the PPh_3 ligand, cyclization of the triyne diester proceeds *via* the oxidative coupling between the terminal alkynoate and internal unactivated alkyne moieties, producing a palladacyclopentadiene with a coordinated alkyne. The palladacyclopentadiene is subsequently transformed into a palladacycloheptatriene through the two-step insertion of the pendant alkyne. The final reductive elimination generates an η^2-arene complex with high exergonicity. In contrast, in the presence of the PPh_3 ligand, the initial oxidative coupling occurs more easily to produce a similar palladacyclopentadiene intermediate, which undergoes the intramolecular Diels–Alder reaction with a non-coordinated alkynoate moiety to directly afford an η^2-arene complex with higher exergonicity. Thus, the PPh_3 ligand considerably facilitates the cyclization of the triyne diester.

Furthermore, the elusive [2+2+2] cycloaddition of diyne diester with nitriles, leading to bicyclic pyridines, was also investigated

WILEY-VCH

to assess its feasibility. The results of the analysis show that the Diels–Alder-type pathway involving two electron-deficient cyanoformate molecules should be feasible under the relevant experimental conditions.

Acknowledgements

This research is partially supported by the Platform Project for Supporting Drug Discovery and Life Science Research (Basis for Supporting Innovative Drug Discovery and Life Science Research (BINDS) from AMED under Grant Number JP20am0101099).

Keywords: alkyne • cycloaddition • benzene • density functional theory calculation • palladium

[1] a) W. Reppe, O. Schlichting, K. Klager, T. Toepel, *Liebigs Ann. Chem.* **1948**, *560*, 1-92; b) W. Reppe, O. Schlichting, H. Meister, *Liebigs Ann. Chem.* **1948**, *560*, 93-104; c) W. Reppe, W. J. Schweckendiek, *Liebigs Ann. Chem.* **1948**, *560*, 104-116.

[2] Selected general reviews: a) S. Saito, Y. Yamamoto, *Chem. Rev.* **2000**, *100*, 2901-2915; b) Y. Yamamoto, *Curr. Org. Chem.* **2005**, *9*, 503-519; c) P. R. Chopade, J. Louie, *Adv. Synth. Catal.* **2006**, *348*, 2307-2327; d) N. Agenet, O. Buisine, F. Slowinski, V. Gandon, C. Aubert, M. Malacria, *Org. React.* **2007**, *68*, 1-302; e) G. Domínguez, J. Pérez-Castells, *Chem. Soc. Rev.* **2011**, *40*, 3430-3444; f) D. L. J. Broere, E. Ruijiter, *Synthesis* **2012**, *44*, 2639-2672; g) Transition-Metal-Mediated Aromatic Ring Construction, Ed. by K. Tanaka, john Wiley & Sons, Hoboken, 2013; h) S. Kotha, K. Lahiri, G. Sreevani, *Synlett* **2018**, *29*, 2342-2361.

[3] A. Roglans, A. Pla-Quintana, M. Solà, *Chem. Rev.* DOI: 10.1021/acs.chemrev.0c00062.

[4] N. E. Shore, *Chem. Rev.* **1988**, *88*, 1081-1119.

[5] a) J. H. Hardesty, J. B. Koerner, T. A. Albright, G.-Y. Lee, *J. Am. Chem. Soc.* **1999**, *121*, 6055-6067; b) A. A. Dahy, N. Koga, *Bull. Chem. Soc. Jpn.* **2005**, *78*, 781-791; c) A. A. Dahy, C. H. Suresh, N. Koga, *Bull. Chem. Soc. Jpn.* **2005**, *78*, 792-803; d) N. Agenet, V. Gandon, K. P. C. Vollhardt, M. Malacria, C. Aubert, *J. Am. Chem. Soc.* **2007**, *129*, 8860-8871.

[6] a) L. Orian, J. N. P. van Stralen, F. M. Bickelhaupt, *Organometallics* **2007**, *26*, 3816-3830; b) A. Dachs, S. Osuna, A. Roglans, M. Solà, *Organometallics* **2010**, *29*, 562-569.

[7] a) K. Kirchner, M. J. Calhorda, R. Schmidt, L. F. Veiros, *J. Am. Chem. Soc.* **2003**, *125*, 11721-11729; b) Y. Yamamoto, T. Arakawa, R. Ogawa, K. Itoh, *J. Am. Chem. Soc.* **2003**, *125*, 12143-12160.

[8] a) M. O. Albers, D. J. A. de Waal, D. C. Liles, D. J. Robinson, E. Singleton, M. B. Wiege, *J. Chem. Soc., Chem. Commun.* **1986**, 1680-1682; b) C. Ernst, O. Walter, E. Dinjus, S. Arzberger, H. Görls, *J. Prakt. Chem.* **1999**, *341*, 801-804; c) Y. Yamada, J. Mizutani, M. Kurihara, H. Nishihara, *J. Organomet. Chem.* **2001**, *637–639*, 80-83; d) Y. Yamamoto, K. Hata, T. Arakawa, K. Itoh, *Chem. Commun.* **2003**, 1290-1291; e) B. Dutta, B. F. E. Curchod, P. Campomanes, E. Solari, R. Scopelliti, U. Rothlisberger, K. Severin, *Chem. Eur. J.* **2010**, *16*, 8400-8409.

[9] M. Paneque, M. L. Poveda, N. Rendón, K. Mereiter, *J. Am. Chem. Soc.* **2004**, *126*, 1610-1611.

[10] Selected examples: a) H. Dietl, H. Reinheimer, J. Moffat, P. M. Maitlis, *J. Am. Chem. Soc.* **1970**, *92*, 2276-2285; b) E. Negishi, L. S. Harring, Z. Owczarczyk, M. M. Mohamud, M. Ay, *Tetrahedron Lett.* **1992**, *33*, 3253-3256; c) J. Li, H. Jiang, M. Chen, *J. Org. Chem.* **2001**, *66*, 3627-3629; d) I. Ojima, A. T. Vu, J. V. McCullagh, A. Kinoshita, *J. Am. Chem. Soc.* **1999**, *121*, 3230-3231; e) C. B. Provis-Evans, S. Lau, V. Krewald, R. L. Webster, *ACS Catal.* **2020**, *10*, 10157-10168.

[11] Selected examples: a) J.-U. Peters, S. Blechert, *Chem. Commun.* **1997**, 1983-1984; b) S. K. Das, R. Roy, *Tetrahedron Lett.* **1999**, *40*, 4015-4018; c) B. Witulski, T. Stengel, J. M. Fernández-Hernández, *Chem. Commun.* **2000**, 1965-1966; d) G. B. Hoven, J. Efskind, C. Rømming, K. Undheim, *J. Org. Chem.* **2002**, *67*, 2459-2463; e) Á. Mallagaray, S. Medina, G. Domínguez, J. Pérez-Castells, *Synlett* **2010**, 2114-2118.

[12] a) K. Moseley, P. M. Maitlis, *Chem. Commun.* **1971**, 1604-1605; b) K. Moseley, P. M. Maitlis, *J. Chem. Soc. Dalton* **1974**, 169-175; c) TS. Ito, S. Hasegawa, Y. Takahashi, Y. Ishii, *J. Organomet. Chem.* **1974**, *73*, 401-409. Also, see: d) H. tom Dieck, C. Munz, C. Müller, *J. Organomet. Chem.* **1990**, *384*, 243-255.

[13] a) Y. Yamamoto, A. Nagata, K. Itoh, *Tetrahedron Lett.* **1999**, *40*, 5035-5038; b) Y. Yamamoto, A. Nagata, Y. Arikawa, K. Tatsumi, K. Itoh, *Organometallics* **2000**, *19*, 2403-2405; c) Y. Yamamoto, A. Nagata, H. Nagata, Y. Ando, Y. Arikawa, K. Tatsumi, K. Itoh, *Chem. Eur. J.* **2003**, *9*, 2469-2483.

[14] Gaussian 16, Revision B.01, M. J. Frisch, G. W. Trucks, H. B. Schlegel, G. E. Scuseria, M. A. Robb, J. R. Cheeseman, G. Scalmani, V. Barone, G. A. Petersson, H. Nakatsuji, X. Li, M. Caricato, A. V. Marenich, J. Bloino, B. G. Janesko, R. Gomperts, B. Mennucci, H. P. Hratchian, J. V. Ortiz, A. F. Izmaylov, J. L. Sonnenberg, D. Williams-Young, F. Ding, F. Lipparini, F. Egidi, J. Goings, B. Peng, A. Petrone, T. Henderson, D. Ranasinghe, V. G. Zakrzewski, J. Gao, N. Rega, G. Zheng, W. Liang, M. Hada, M. Ehara, K. Toyota, R. Fukuda, J. Hasegawa, M. Ishida, T. Nakajima, Y. Honda, O. Kitao, H. Nakai, T. Vreven, K. Throssell, J. A. Montgomery, Jr., J. E. Peralta, F. Ogliaro, M. J. Bearpark, J. J. Heyd, E. N. Brothers, K. N. Kudin, V. N. Staroverov, T. A. Keith, R. Kobayashi, J. Normand, K. Raghavachari, A. P. Rendell, J. C. Burant, S. S. Iyengar, J. Tomasi, M. Cossi, J. M. Millam, M. Klene, C. Adamo, R. Cammi, J. W. Ochterski, R. L. Martin, K. Morokuma, O. Farkas, J. B. Foresman, and D. J. Fox, Gaussian, Inc., Wallingford CT, 2016.

[15] a) A. D. Becke, *J. Chem. Phys.* **1993**, *98*, 5648-5652; b) J. P. Perdew, Y. Wang, *Phys. Rev. B* **1992**, *45*, 13244-13249.

[16] a) P. J. Hay, W. R. Wadt, *J. Chem. Phys.* **1985**, *82*, 299-310; b) A. W. Ehlers, M. Böhme, S. Dapprich, A. Gobbi, A. Höllwarth, V. Jonas, K. F. Köhler, R. Stegmann, A. Veldkamp, G. Frenking, *Chem. Phys. Lett.* **1993**, *208*, 111-114.

[17] a) W. J. Hehre, R. Ditchfield, J. A. Pople, *J. Chem. Phys.* **1972**, *56*, 2257-2261; b) P. C. Hariharan, J. A. Pople, *Theor. Chim. Acta* **1973**, *28*, 213-222; c) M. M. Fracl, W. J. Pietro, W. J. Hehre, J. S. Binkley, M. S. Gordon, D. J. DeFrees, J. A. Pople, *J. Chem. Phys.* **1982**, *77*, 3654-3665.

[18] S. Grimme, S. Ehrlich, L. Goerigk, *J. Comp. Chem.* **2011**, *32*, 1456-1465.

[19] a) K. Fukui, *Acc. Chem. Res.* **1981**, *14*, 363-368; b) C. Gonzalez, H. B. Schlegel, *J. Chem. Phys.* **1989**, *90*, 2154-2161; c) C. Gonzalez, H. B. Schlegel, *J. Phys. Chem.* **1990**, *94*, 5523-5527.

[20] a) D. Andrae, U. Häussermann, M. Dolg, H. Stoll, H. Preuß, *Theor. Chim. Acta* **1990**, *77*, 123-141; b) J. M. L. Martin, A. Sundermann, *J. Chem. Phys.* **2001**, *114*, 3408-3420.

[21] a) R. Krishnan, J. S. Binkley, R. Seeger, J. A. Pople, *J. Chem. Phys.* **1980**, *72*, 650-654; b) A. D. McLean, G. S. Chandler, *J. Chem. Phys.* **1980**, *72*, 5639-5648; c) M. J. Frisch, J. A. Pople, J. S. Binkley, *J. Chem. Phys.* **1984**, *80*, 3265-3269; d) T. Clark, J. Chandrasekhar, G. W. Spitznagel, P. v. R. Schleyer, *J. Comp. Chem.* **1983**, *4*, 294-301.

[22] A. V. Marenich, C. J. Cramer, D. G. Truhlar, *J. Phys. Chem. B* **2009**, *113*, 6378-6396.

[23] Legault, C. Y., Université de Sherbrooke, 2009 (http://www.cylview.org).

[24] It is likely that the barriers for the initial oxidative coupling are somewhat overestimated, see: G. T. De Jong, D. P. Geerke, A. Diefenbach, M. Solà, F. M. Bickelhaupt, *J. Comput. Chem.* **2005**, *26*, 1006-1020.

[25] M. Wakioka, Y. Nakajima, F. Ozawa, *Organometallics* **2009**, *28*, 2527-2534.

[26] Selected reviews: a) J. A. Varela, C. Saá, *Chem. Rev.* **2003**, *103*, 3787-3801; b) B. Heller, M. Hapke, *Chem. Soc. Rev.* **2007**, *36*, 1085-1094; c) J. A. Varela, C. Saá, *Synlett* **2008**, 2571-2578.

[27] a) H. Bönnemann, R. Brinkmann, H. Schenkluhn, *Synthesis* **1974**, 575-577; b) H. Bönnemann, R. Brinkmann, *Synthesis* **1975**, 600-602; c) Y. Wakatsuki, H. Yamamzaki, *Tetrahedron Lett.* **1975**, 3383-3384; d) Y. Wakatsuki, H. Yamamzaki, *Synthesis* **1976**, 26-28.

[28] a) S. P. Mulcahy, J. G. Varelas, *Tetrahedron Lett.* **2013**, *54*, 6599-6601; b) B. M. Saliba, S. Khanal, M. A. O'Donnell, K. E. Queenan, J. Song, M. R. Gentile, S. P. Mulcahy, *Tetrahedron Lett.* **2018**, *59*, 4311-4314; c) K. M. Medas, R. W. Lesch, F. B. Edioma, S. P. Wrenn, V. Ndahayo, S. P. Mulcahy, *Org. Lett.* **2020**, *22*, 3135-3139.

[29] a) B. N. Storhoff, H. C. Lewis, Jr., *Coord. Chem. Rev.* **1977**, *23*, 1-29; b) R. A. Michelin, M. Mozzon, R. Bertani, *Coord. Chem. Rev.* **1996**, *147*, 299-338; c) N. A. Bokach, V. Y. Kukushkin, *Coord. Chem. Rev.* **2013**, *257*, 2293-2316.

WILEY-VCH

Entry for the Table of Contents

Insert graphic for Table of Contents here. ((Please ensure your graphic is in **one** of following formats))

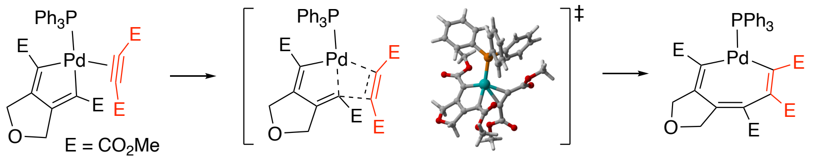

DFT study of Pd(0)-catalyzed [2+2+2] cocycloaddition

The mechanisms of the palladium(0)-catalyzed cross [2+2+2] cycloaddition of a diyne diester with dimethyl acetylenedicarboxylate and of the [2+2+2] cyclization of a triyne diester were investigated using density functional theory calculations. The roles of the ester substituents on the alkyne substrates and of the triphenylphosphine ligand are discussed based on the obtained results.

Key Topic: [2+2+2] Cycloaddition

Institute and/or researcher Twitter usernames: @YamamotoLab1

WILEY-VCH